Giant Magnetic In-Plane Anisotropy and Competing Instabilities in $Na_3Co_2SbO_6$

Xintong Li,[1,*,†] Yuchen Gu,[1,†] Yue Chen,[1,†] V. Ovidiu Garlea,[2] Kazuki Iida,[3] Kazuya Kamazawa,[3] Yangmu Li,[4,5,6] Guochu Deng,[7] Qian Xiao,[1] Xiquan Zheng,[1] Zirong Ye,[1] Yingying Peng,[1,8] I. A. Zaliznyak,[5,‡] J. M. Tranquada,[5] and Yuan Li[1,8,§]

[1]*International Center for Quantum Materials, School of Physics, Peking University, Beijing 100871, China*
[2]*Neutron Scattering Division, Oak Ridge National Laboratory, Oak Ridge, Tennessee 37831, USA*
[3]*Neutron Science and Technology Center, Comprehensive Research Organization for Science and Society, Tokai, Ibaraki 319-1106, Japan*
[4]*Beijing National Laboratory for Condensed Matter Physics, and Institute of Physics, Chinese Academy of Sciences, Beijing 100190, China*
[5]*Condensed Matter Physics and Materials Science Division, Brookhaven National Laboratory, Upton, New York 11973, USA*
[6]*School of Physical Sciences, University of Chinese Academy of Sciences, Beijing 100049, China*
[7]*Australian Centre for Neutron Scattering, Australian Nuclear Science and Technology Organisation, Lucas Heights, New South Wales 2234, Australia*
[8]*Collaborative Innovation Center for Quantum Matter, Beijing 100871, China*

(Received 14 April 2022; revised 26 August 2022; accepted 10 October 2022; published 2 December 2022)

We report magnetometry data obtained on twin-free single crystals of $Na_3Co_2SbO_6$, which is considered a candidate material for realizing the Kitaev honeycomb model for quantum spin liquids. Contrary to a common belief that such materials can be modeled with the symmetries of an ideal honeycomb lattice, our data reveal a pronounced twofold symmetry and in-plane anisotropy of over 200%, despite the honeycomb layer's tiny orthorhombic distortion of less than 0.2%. We further use magnetic neutron diffraction to elucidate a rich variety of field-induced phases observed in the magnetometry. These phases manifest themselves in the paramagnetic state as diffuse scattering signals associated with competing ferromagnetic and antiferromagnetic instabilities, consistent with a theory that also predicts a quantum spin liquid phase nearby. Our results call for theoretical understanding of the observed in-plane anisotropy and render $Na_3Co_2SbO_6$ a promising ground for finding exotic quantum phases by targeted external tuning.

DOI: 10.1103/PhysRevX.12.041024

Subject Areas: Condensed Matter Physics, Magnetism, Strongly Correlated Materials

I. INTRODUCTION

Frustrated magnetic systems have the potential to realize exotic quantum spin liquids (QSLs) [1–3]. The exactly solvable Kitaev model [4], which features bond-dependent Ising interactions between effective spin-1/2 nearest neighbors on a honeycomb lattice, has motivated intensive QSL research in recent years. As a guiding principle, it is believed that such interactions can be realized in spin-orbit-coupled Mott insulators [5–8]. Solid-state platforms for realizing the Kitaev model have evolved over the years from 5*d* iridium [9] to 4*d* ruthenium [10] compounds and, most recently, to 3*d* cobaltates [11–15]. Despite a potential drawback of weaker spin-orbit coupling, the cobaltates are believed to have relatively weak non-Kitaev and further-neighbor interactions compared to their 4*d* and 5*d* counterparts [11,12,15].

As a reality of nature, essentially all candidate Kitaev magnets have long-range order at low temperatures [6,16–20]. This is attributed to the presence of interactions beyond the Kitaev model [9,21–30], such that additional tuning is needed to overcome the ordering tendency, e.g., by using thermal disorder and external fields [13,31–37], in order to recover QSL behaviors. To this end, it is important to know how close the microscopic model of a given system is to an anticipated QSL phase. The cobaltate $Na_3Co_2SbO_6$ is promising in this regard, as its model is inferred to situate near boundaries between ferromagnetic (FM), antiferromagnetic (AFM), and QSL phases [13]. This understanding is supported by the

*xintongli@iphy.ac.cn
†These authors contributed equally to this work.
‡zaliznyak@bnl.gov
§yuan.li@pku.edu.cn

relatively low Néel temperature (T_N) and small saturation fields of the system compared to its sister compound $Na_2Co_2TeO_6$ [16,38–40].

Notably, while non-Kitaev and further-neighbor terms are widely considered in theoretical constructions [21,23–30,41–45], the low, monoclinic symmetry of many candidate materials, including Na_2IrO_3 [17,18], α-$RuCl_3$ [19,46], and $Na_3Co_2SbO_6$ [16], is often neglected. Even though originating from interlayer stacking, the monoclinicity also means lack of C_3 rotational symmetry of the crystal field and a transition-metal ion's interactions with its neighbors in the same layer. Approximating the interactions with their bond-averaged values [30] is an assumption commonly taken but rarely checked. Two cobaltates, $Na_2Co_2TeO_6$ [16] and $BaCo_2(AsO_4)_2$ [20], have the C_3 symmetry, but their zero-field ground states are reported to be dissimilar to the monoclinic systems [20,47,48], and no consensus has been reached concerning the microscopic models [49–54]. The lack of C_3 symmetry should result in magnetic in-plane anisotropy, as is observed in α-$RuCl_3$ [55]. However, the anisotropy is found to vary considerably [55–57], possibly due to sample-dependent monoclinic domain population.

Here, we report a systematic study of $Na_3Co_2SbO_6$ aided by the use of twin-free crystals. Magnetometry reveals at low temperatures a strong C_2 in-plane anisotropy, in both the low-field susceptibility and the critical fields for switching toward a series of field-induced states. The magnitude of the anisotropy is unprecedented, yet the field-induced transitions resemble other systems to some extent. We further use neutron diffraction to determine the wave vectors of the field-induced states. They signify a series of AFM and FM instabilities, which closely compete and produce distinct diffuse scattering above T_N in zero field. These results render $Na_3Co_2SbO_6$ a highly intriguing system with the potential to realize exotic phases under targeted tuning.

II. MAGNETOMETRY ON TWIN-FREE CRYSTALS

Figures 1(a) and 1(b) present the crystal and reciprocal-space structure, respectively, of $Na_3Co_2SbO_6$, which has the same space group ($C2/m$) as α-$RuCl_3$ [19,46]. A peculiarity common to both structures is in the stacking: Adjacent honeycomb layers are offset from each other by $-\mathbf{a}/3$; hence, we have $a/c \approx -3\cos\beta$, with $[a, b, c] = [5.371, 9.289, 5.653]$ Å and $\beta = 108.6°$ in $Na_3Co_2SbO_6$ [39]. Similar to α-$RuCl_3$ [46], the orthorhombic distortion in the honeycomb layer of $Na_3Co_2SbO_6$ is tiny: The distortion is measured as $\sqrt{3}a/b - 1 < 0.002$ [39,40]. Yet, we find that such a small distortion removes the overall S_6 and C_3 symmetries. We next show the far-reaching consequences on the magnetism using a rare growth product: twin-free single crystals. Such crystals can be found by screening with Raman spectroscopy (Fig. S1 in Ref. [58]) and ultimately verified with x-ray diffraction [Fig. 1(c)]. They have a well-defined T_N of about 6.6 K (Fig. S2 in Ref. [58]) with sample-dependent variation of no more than 1 K possibly caused by structural imperfections. The variation is considerably smaller than in the literature [16,38–40]. This is in line with the facts that our best crystals have very few stacking faults [Fig. 1(c)] compared to a previous report [39] and that the observed Bragg intensities agree well with calculation based on the ideal crystal structure [Fig. 1(d)]. Our further refinement attempts suggest that the agreement cannot be improved

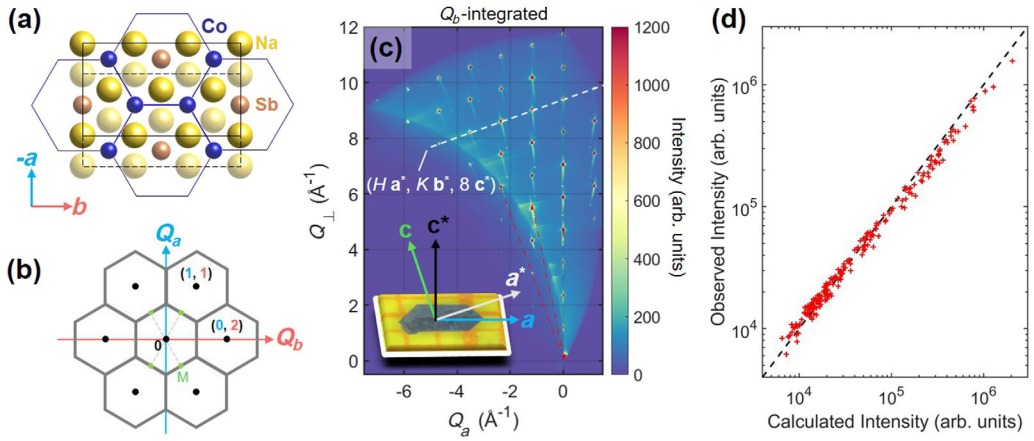

FIG. 1. (a) Unit cell of $Na_3Co_2SbO_6$ viewed from the top perpendicular to the ab plane, omitting oxygen atoms. The solid (dashed) rectangle indicates cell boundary in the top (bottom) Na layer. Hexagons indicate the Co sublattice in the middle layer. (b) Two-dimensional (2D) structural Brillouin zones, indexed in units of a^* and b^* projected into the ab plane. Zone centers (Γ points) are $Q_a + Q_b =$ even, and M points are midpoints between Γ. (c) X-ray diffraction in the a^*c^* plane, obtained on a twin-free crystal after integration along $\mathbf{b}^*$. The data can be indexed in a monoclinic setting without twinning. Radial Bragg tails are due to energy spread of the monochromated x rays. The inset is a photo of a crystal with pertinent axes indicated. (d) Observed x-ray diffraction intensities from 204 indexed Bragg peaks compared to calculation from the ideal crystal structure.

by introducing antisite disorder between Co and Sb [39]. While the data do not allow us to rule out disorder in the Na layers [39], we consider its role to be minor, because such disorder is expected to cause stacking faults which are rare in our crystals.

Figure 2(a) shows how a pronounced **a**-**b** anisotropy develops in the magnetic susceptibility upon cooling. Far above T_N, we observe an approximately 10% anisotropy consistent with the anisotropy of the g factor, $g_b > g_a$ (Figs. S3 and S4 and Table S1 in Ref. [58]), as is also seen from high-field magnetization where moments are nearly polarized [Fig. 2(b)]. The anisotropy drastically increases to over 200% near T_N (see Fig. S3 in Ref. [58] for out-of-plane anisotropy), which signifies the role of the fluctuations—the moments respond much more strongly in the easy direction nearly parallel to the developing order parameter [39]. This understanding also explains why the anisotropy is reversed below T_N. The reversal is no longer observed in $B = 2$ T (Fig. S3 in Ref. [58]), which is large enough to overcome the AFM order. We make two remarks here to relate to previous works: (i) The **a**-axis response clearly drops below T_N [Fig. 2(a)], suggesting that the ordered moments are not entirely along **b** [39]. (ii) No reversal is observed below T_N in α-$RuCl_3$ [55], where the anisotropy also appears to be much weaker.

The competition between anisotropic interactions and the applied field is more clearly seen in the magnetization at 2 K [Figs. 2(b)–2(d)], where our twin-free sample reveals a wealth of remarkable features unnoticed in previous works [16,38–40]. Two well-separated transitions are observed along both **a** and **b**, at critical fields [B_{c1} and B_{c2}, Fig. 2(b)] that again differ strongly between the two directions. The lower-field transition is clearly hysteretic, as indicated by the magnetization's dependence on the field-sweeping direction. It further splits into two hysteretic transitions, the critical fields of which we refer to as $B_{c1,\mathrm{low}}$ and $B_{c1,\mathrm{high}}$, when the field is applied in plane but away from the high-symmetry **a** and **b** axes [Figs. 2(c) and 2(d)]. The lowest $B_{c1,\mathrm{low}}$ value is found at about 15° away from **b**. The highest $B_{c1,\mathrm{high}}$ can approach B_{c2} and become no longer visible from the data, over a range of field directions between 10° and 30° away from **a**. Hence, very unexpectedly, there is nearly no sixfold symmetry in the results, including in the nearly field-polarized state at 2 T (Fig. S3 in Ref. [58]). The large magnitude of **a**-**b** anisotropy sharply contrasts with the C_3-symmetric sister compound

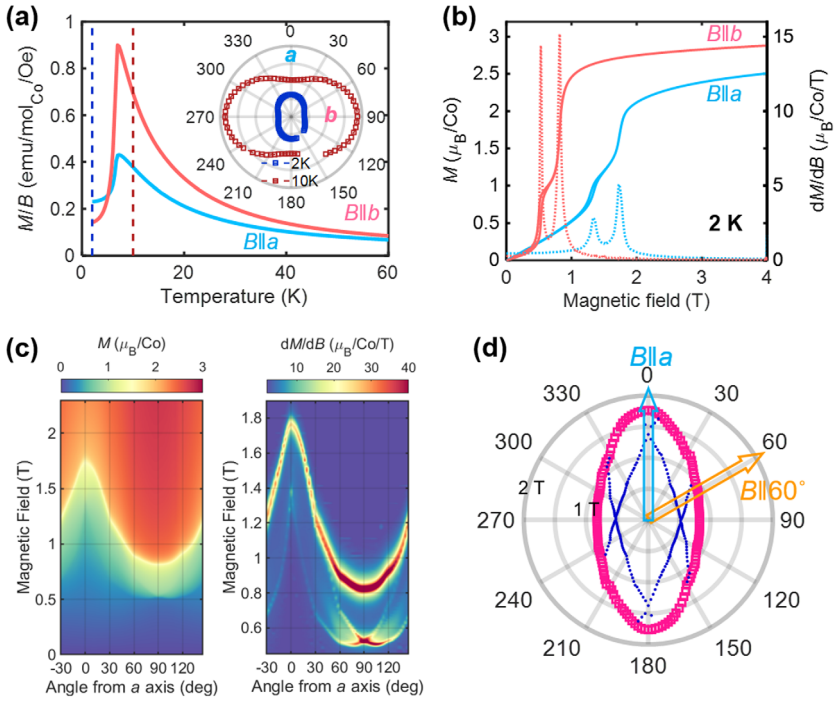

FIG. 2. (a) dc magnetic susceptibility measured in fields of 0.1 T along the **a** and **b** axes. The inset displays the susceptibility versus in-plane angle at 2 and 10 K (dashed lines in the main panel), showing highly pronounced C_2 profiles which reverse the long and short axes across T_N. (b) Magnetization versus field data (solid lines) reveal two transitions along both **a** and **b** at 2 K. The critical fields (B_{c1} and B_{c2}) are determined from the derivative (dashed lines) as (0.82, 1.76 T) for **a** and (0.52, 1.37 T) for **b**, with an uncertainty of ±0.02 T. Data are displayed for both field-up and -down sweeping directions, which are nearly identical except near B_{c1}, indicating a hysteretic nature of the transition. (c) In-plane angle dependence of magnetization versus field (left) and the field derivative (right) at 2 K. Measurement at each angle is performed over a field-up sweep, and the field is decreased to zero before moving to the next angle. It is seen that B_{c1} splits away from **a** and **b**. (d) Summary of the result in (c) after 180° symmetrization. Empty arrows are a reference for the field directions in Fig. 4.

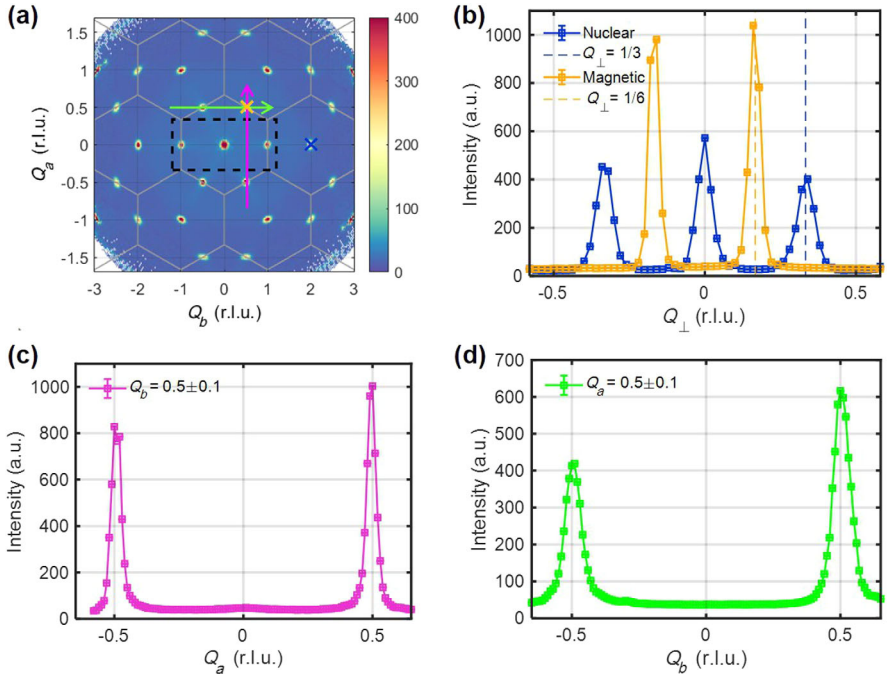

FIG. 3. (a) $Q_\perp$-integrated diffraction data measured at 6 K and in zero field. Gray hexagons indicate 2D Brillouin zones. Color-coded crosses and arrows indicate locations of line cuts in (b)–(d). The dashed box indicates the restricted data coverage in Fig. 4. (b) Line cuts along $Q_\perp$ through nuclear and magnetic Bragg peaks. The nuclear peaks at $Q_\perp = 0$ and $\pm 1/3$ are contributed by physical reflections $(0, 2\mathbf{b}^*, 0)$ of S_a and $(\mathbf{a}^*, \mathbf{b}^*, 0)$ of S_{60}, respectively. The magnetic peaks at $Q_\perp = \pm 1/6$ are contributed by reflections $(\pm\mathbf{a}^*/2, \pm\mathbf{b}^*/2, 0)$ of both domains. (c),(d) Line cuts along Q_a and Q_b through the magnetic reflections. The map in (a) is symmetrized, whereas the line cuts in (b)–(d) are not symmetrized.

$Na_2Co_2TeO_6$, where the magnetic responses along **a** and $\mathbf{a}^*$ are reasonably similar [37,50]. We note that quenched disorders may play a role in the experimentally observable anisotropy in $Na_3Co_2SbO_6$. By heating up a twin-free crystal to 600 °C at 20 °C/ min, staying for 1 h, and quenching the crystal in liquid nitrogen, we find the susceptibility anisotropy ratio [χ_b/χ_a; see Fig. 2(a)] to change from 1.81 to 1.78 at 10 K and from 0.53 to 0.75 at 2 K. The two field-induced transitions [Fig. 2(b)] at 2 K also become considerably smeared out. According to x-ray diffraction, the crystal remains twin-free after the quenching.

III. MAGNETIC NEUTRON DIFFRACTION

We next turn to the intermediate state(s) between B_{c1} and B_{c2}. While the steplike and hysteretic (near B_{c1}) behaviors hint at a spin-flop origin [16,38–40], our observation of the transitions along both **a** and **b** (and everywhere in between) defies such an interpretation. The result in Fig. 2(c) is furthermore independent of field or temperature history, precluding the relevance of magnetic domain repopulation [34,64]. Motivated by the fact that the magnetization above B_{c1} resembles "plateau" phases found in low-dimensional frustrated magnets [65–68]—i.e., it reaches about $1/3$ and $1/2$ of saturation [Fig. 2(b)] for $B_{\|b}$ and $B_{\|a}$, respectively—we perform neutron diffraction in magnetic fields to explore this possibility. The experiment is done on a coaligned but twinned array of crystals with their $\mathbf{c}^*$ axis horizontal, such that the vertical field is along **a** for $1/3$ of the sample (S_a) and at 60° from **a** for the rest (S_{60}); see illustrations in the upper-left corner in Fig. 4. In spite of the twinning, there is no ambiguity in the domain origin (S_a or S_{60}) of the field-evolving signals, under the assumption that magnetization and diffraction see the same transitions (Fig. S5 in Ref. [58]). According to magnetization [Fig. 2(d)], all transitions occur below (above) 1 T for S_{60} (S_a). The difference is illustrated by the thick horizontal arrow diagrams in the upper half of Fig. 4.

We use here a "hybrid" orthogonal coordinate system for the reciprocal space, illustrated in Fig. 1(b). Wave vectors are denoted as $(Q_a, Q_b, Q_\perp)$, with Q_b and $Q_\perp$ in units of $\mathbf{b}^*$ and $\mathbf{c}^*$, respectively. Q_a is in units of $\mathbf{a}^*$ projected onto the real-space **a** axis, and it is parallel to the vertical field. This coordinate system is convenient for describing a twinned sample, because the twinning features C_6 rotations within the ab plane and mixes up Q_a and Q_b while leaving $Q_\perp$ intact. We write $\mathbf{a}^*$, $\mathbf{b}^*$, and $\mathbf{c}^*$ explicitly when we refer to the (physical) monoclinic indices. A table reference for transforming between the two indexing systems can be found in Table S3 [58]. To give some examples, nuclear Bragg peaks at $(0, 2, \pm 1/3)$ in the hybrid notation [Figs. 3(a) and 3(b)] are associated with physical indices $(\pm\mathbf{a}^*, \pm\mathbf{b}^*, 0)$ of S_{60}. In zero field, the AFM wave vectors

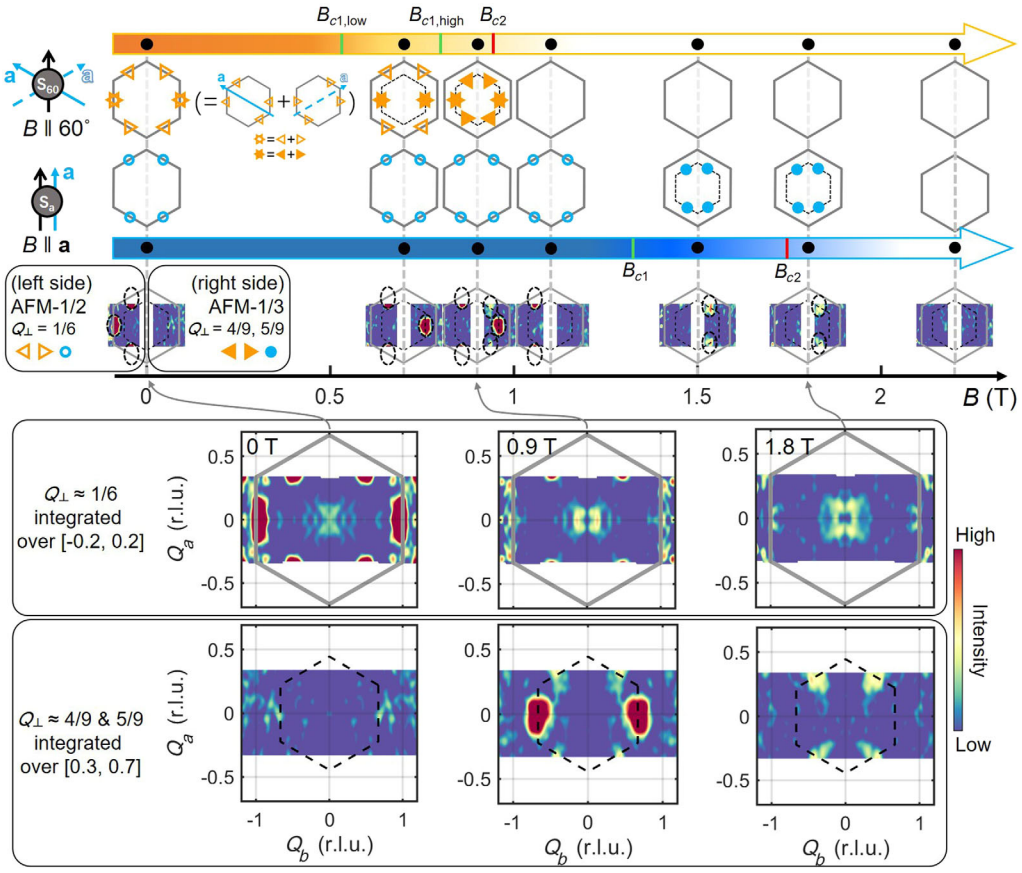

FIG. 4. The upper half illustrates the behavior of two sample parts (S_a or S_{60}; see legends on the left and text) as the field passes through their respective phase boundaries [Fig. 2(d)]. S_a is uniquely defined as per the in-plane orientation, and it contributes diffractions indicated by blue circles. S_{60} further contains two parts that are related by 180° rotation about the field, which contribute diffractions indicated by left- and right-pointing orange triangles. Empty and filled symbols indicate AFM $\frac{1}{2}$ and AFM $\frac{1}{3}$ wave vectors (see the text), respectively, which are measured by restricting $Q_\perp$ to $[-0.2, 0.2]$ and $[0.3, 0.7]$, respectively. Miniatures of diffraction data (measured at $T = 0.25$ K) are displayed in the bottom row of the illustration in a left-right split fashion, where the observed diffraction peaks (encircled by dashed ellipses centered at their expected locations, some of which fall beyond the data coverage) are fully consistent with the "$S_a + S_{60}$" combination of the cartoons. Solid and dashed hexagons are the first Brillouin zone and 2/3 of it, respectively. In the lower half, we display diffraction data measured at three selected fields, where the solid and dashed hexagons have the same meaning as in the upper-half illustration. Note that the vertical ($\|Q_a$) data coverage is limited and the resolution is relatively poor compared to those in Fig. 3. An animated view of the full variable-field data is presented in Fig. S10 in Ref. [58].

$(\pm\mathbf{a}^*/2, \pm\mathbf{b}^*/2, 0)$ [39] of S_a transform into $(\pm 0.5, \pm 0.5, \pm 1/6)$ in the hybrid notation [Figs. 3(b)–3(d)], producing diffractions at four (Q_a, Q_b) locations, whereas the same diffractions from the two copies of S_{60} (Fig. 4) are expected at six (Q_a, Q_b) locations. All of these AFM wave vectors have $|Q_\perp| = 1/6$ as indicated by empty symbols in Fig. 4. While the data coverage in Fig. 4 along the Q_a direction is limited compared to that in Fig. 3, magnetic diffractions above and below the $Q_a = 0$ (horizontal) plane are partly observed. This is enabled by vertical focusing optics [58], which relaxes the momentum resolution and elongates diffraction features in the Q_a direction.

The results in Fig. 4 can be summarized as follows: The AFM wave vectors switch from $(\pm\mathbf{a}^*/2, \pm\mathbf{b}^*/2, 0)$ at $B = 0$ to $(\pm\mathbf{a}^*/3, \pm\mathbf{b}^*/3, \pm\mathbf{c}^*/3)$ above B_{c1}, and eventually no AFM is left above 2.2 T (see methods section and Figs. S5–S7 in Ref. [58] for additional evidence for the peak indexing). We, therefore, refer to the zero-field and the intermediate states as AFM $\frac{1}{2}$ and AFM $\frac{1}{3}$, respectively. The AFM $\frac{1}{3}$ wave vectors all have $Q_\perp = 4/9$ or $5/9$ [58], which allows the diffraction peaks to be observed separately from the AFM $\frac{1}{2}$ ones by restricting $Q_\perp$ in the experiment (Fig. 4). Notably, due to the low-symmetry field direction for S_{60}, the wave vectors in this part of the sample do not switch together. Instead, the switching occurs in two steps for the diffraction peaks situated on different Γ-M lines [Fig. 1(b)] relative to the field; see the comparison of the 0, 0.7, and 0.9 T illustrations for S_{60} and the associated data in the upper half of Fig. 4. This two-step switching behavior is fully consistent with the two transitions at $B_{c1,low}$ and $B_{c1,high}$ for the same field direction, which we

establish with magnetometry [Fig. 2(d)]. We note that, at each transition, the switching wave vectors remain on the same Γ-M lines, without intermixing between the 2D momentum directions.

The wave-vector switch supports the idea that AFM $\frac{1}{3}$ is a ferrimagnetic phase with an enlarged 2D cell compared to AFM $\frac{1}{2}$, such as "↑↑↓" compared to "↑↓." With the understanding that AFM $\frac{1}{2}$ features zigzag order [39], which consists of alternating FM chains running along zigzag lines of the honeycomb lattice, AFM $\frac{1}{3}$ could feature alternating wide and narrow FM ribbons and chains. An illustration of such FM chains without the alternating correlation can be found in Fig. 6(a). The two-step transitions of B_{c1} and the single-step transition of B_{c2} introduce some restrictions on the magnetic structure, which we discuss in Ref. [58]. We further note that B_{c2} does *not* necessarily mark entrance into a field-polarized state, certainly not for S_a, since the AFM $\frac{1}{3}$ diffraction peaks persist above B_{c2} (Fig. 4). The nature of B_{c2} will be reported elsewhere. Further above B_{c2}, all magnetic diffraction eventually coincide with nuclear Bragg peaks, as expected for a field-polarized state.

Taken together, the results show that at very low T and in external in-plane fields, $Na_3Co_2SbO_6$ sequentially goes through magnetic states characterized by the M point, the "$\frac{2}{3}M$" point, and eventually the zone-center Γ point, forming an evolution along the Γ-M lines [Fig. 1(b)]. The direction of the field affects only when, but not whether, the transitions occur. It is, therefore, tempting to think that the system possesses competing AFM-FM instabilities with wave vectors lined up along Γ-M. In Fig. 5, we use variable-T neutron diffraction to show that this is indeed the case. The experiment is performed on a twinned sample, in *zero* magnetic field. The most remarkable observation is found at 10 K [Fig. 5(c)]: We see distinct hexagonal-star-shaped diffuse scattering, which "flows" into the long-range magnetic Bragg peaks at the M points upon further cooling [Fig. 5(b)]. The observed star consists of six narrow streaks which precisely cover the Γ-M lines. In a twin-free sample, the number of streaks would likely be four [Fig. 1(b)], which would help explain the giant in-plane magnetic anisotropy, and it warrants further experimental confirmation. The streaks are, in fact, quasi-2D objects in reciprocal space with only weak dependence on $Q_\perp$ (Fig. S8 in Ref. [58]). They correspond to quasi-1D correlations in real space (Fig. 6, further discussed below) and can be viewed as a counterpart of rodlike diffuse scattering in $Yb_2Ti_2O_7$ [69,70], which is attributed to coexisting FM and AFM correlations [71,72]. Below T_N, the body of the star is depleted, including the FM-like diffuse scattering near Γ [Fig. 5(a)]. Such a temperature evolution, together with the field evolution at low T (Fig. 4), signifies a close competition between a variety of AFM and FM instabilities, with or without thermal disorder. Indeed, the M-point AFM order might be energetically favored in zero field by only a small margin. We further find evidence for a weak field-trainable net moment in a twin-free sample (Fig. S9 in Ref. [58]), which supports an incipience of the ferromagnetism.

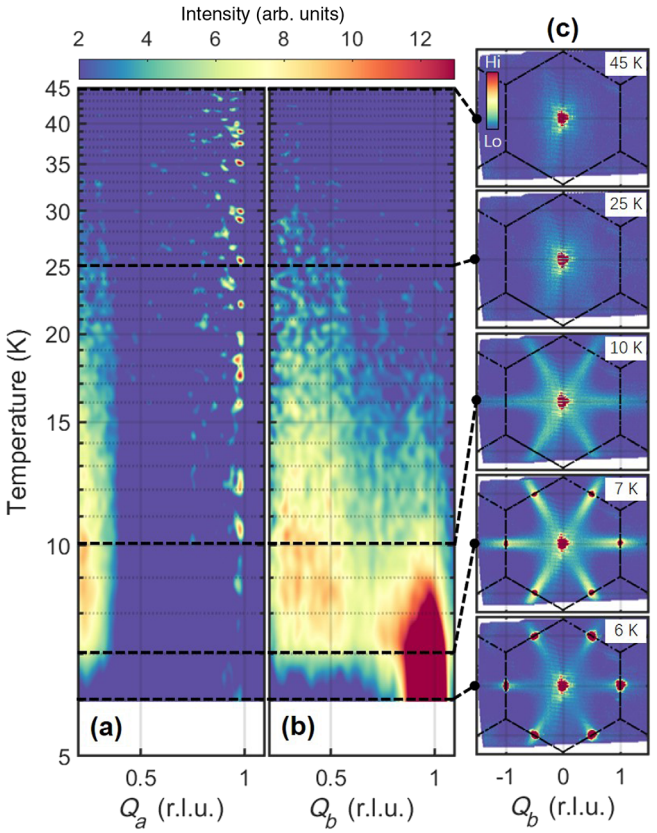

FIG. 5. (a),(b) Variable-T diffuse magnetic scattering in zero field, viewed along Q_a and Q_b starting from near the Γ point, after subtracting the $T = 45$ K data as background. (c) Scattering in the 2D Brillouin zone at selected temperatures. Unlike the nuclear (Γ-point) and magnetic (M-point) Bragg peaks, the diffuse scattering does not show noticeable $Q_\perp$ dependence, and the displayed data are $Q_\perp$ integrated and restricted to a small energy window of ±0.2 meV.

IV. DISCUSSION

Our results motivate further exploration of exotic quantum phases in $Na_3Co_2SbO_6$, as well as in extended Kitaev and related theoretical models. Magnetic field-induced phases in candidate Kitaev materials have been under intense research in recent years [20,34,37,50,56,73–81], and the magnetization's steplike transitions into and out of the intermediate states in Fig. 2 resemble some of the reports [20,37,56], even though the wave-vector switching behavior might not be the same [20,56]. These results suggest that the candidate materials commonly possess multiple magnetic instabilities—a hallmark of frustration. Our findings are consistent with the view that $Na_3Co_2SbO_6$

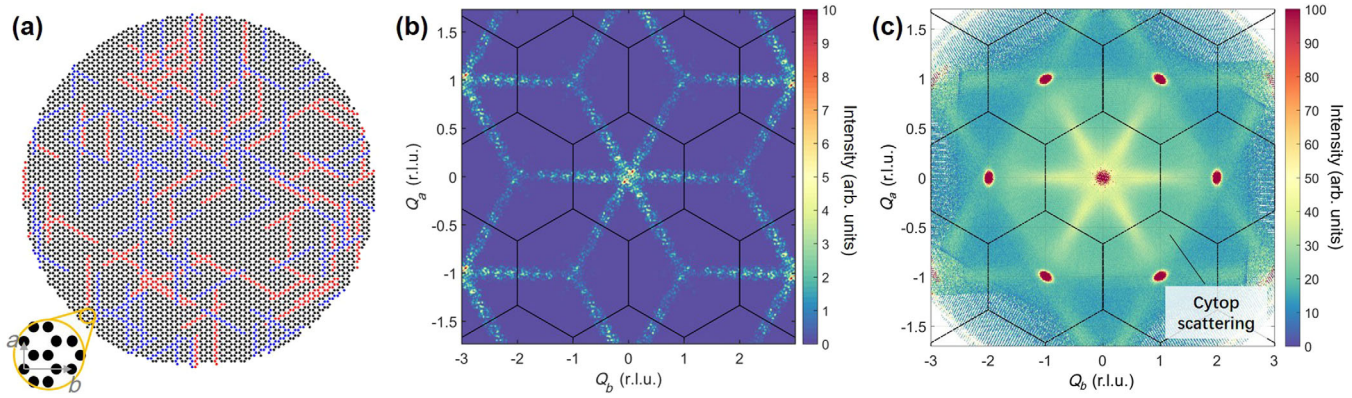

FIG. 6. (a) A random placement of ferromagnetic zigzag chain segments on a honeycomb lattice. Blue, red, and black circles indicate spin-up, spin-down, and spinless sites, respectively, which contribute positive, negative, and zero neutron-scattering amplitudes in the simulation. (b) Fourier component squared of the scattering amplitudes in the field of view in (a), computed on a fine 2D momentum grid. (c) Neutron diffraction intensities at 10 K, similar to those in Fig. 5(c) but acquired with a higher incident energy (Table S2 in Ref. [58]). Data are $Q_\perp$ integrated and are C_6 symmetrized for better comparison with (b). Black hexagons indicate 2D Brillouin zones. Sharp diffraction spots are nuclear Bragg peaks. Halolike diffuse intensities in the first and part of the second zones are T-independent scattering from the sample holder and glue (Cytop).

is close to a trisecting point of FM, AFM, and QSL phases [13], yet the pronounced in-plane anisotropy clearly adds complexity and novelty to the previous understanding. Specifically, given the anisotropy, uniaxial strains both perpendicular [13] and parallel to the honeycomb layers might help promote QSL physics.

Meanwhile, the Γ-M characteristics of the ordering wave vectors and diffuse scattering imply a particular combination of competing instabilities, which are not commonly seen in model systems [45]. In Fig. 6, we show that the star-shaped diffuse scattering pattern can be well simulated by FM zigzag chains randomly placed on a honeycomb lattice. Each star streak in $\mathbf{Q}$ space is contributed by chains in real space that run perpendicular to the streak. Because neutron scattering probes magnetic moments perpendicular to $\mathbf{Q}$, we infer that the magnetic moments in the FM chains point largely parallel to the chains—similar to those in a typical zigzag magnetic structure [18,47]. Given that the AFM order below T_N is preceded by the short-range FM chains above T_N, a plausible scenario is that the system's leading magnetic interactions are strongly in favor of individual FM-chain formation, yet at the same time they are weakly in favor of an alternating side-by-side arrangement of the chains, i.e., *against* the formation of 2D FM order. Together with our inference of the moment direction above, the scenario echoes with the idea of bond-dependent anisotropic interactions, which is at the core of the Kitaev and related models.

We further notice that, among three types of parameters that are commonly considered for explaining the zigzag order [42], our result appears to be consistent with the expected behaviors of models with a leading nearest-neighbor symmetric off-diagonal interaction term, $\Gamma_1 > 0$. This is because, for a given nearest-neighbor pair, the $\Gamma_1 > 0$ term favors FM alignment of the spin component parallel to the bond but AFM alignment of the component perpendicular to both the bond and the Ising axis of the Kitaev term. Together with the geometry of the honeycomb lattice, the $\Gamma_1 > 0$ term can thus explain both the FM chains' formation tendency and their resistance to form 2D FM order. Indeed, in the Appendix in Ref. [42], we find a discussion of such models' several similar behaviors compared to our observations, including the formation of AFM $\frac{1}{3}$ order and competing instabilities at a star-shaped set of wave vectors. Another major feature of such models is their demonstrated ability to produce large magnetic-response anisotropy without a highly anisotropic g tensor [42]. We thus expect our results to motivate further theoretical research of frustrated magnetism in the off-diagonal models [82–84], some of which may have a QSL ground state [84].

In conclusion, we have elucidated the field-induced phases and competing instabilities in the quantum magnet $Na_3Co_2SbO_6$ and uncovered an unexpectedly large magnetic anisotropy. The results indicate exotic magnetic phases and render this system highly promising for further explorations using targeted external tuning. The results also stimulate future theoretical research of spin-orbit-coupled quantum magnets.

ACKNOWLEDGMENTS

We are grateful for technical support by Qizhi Li and Jianping Sun and for discussions with Wenjie Chen, Ji Feng, L. Janssen, G. Khaliullin, V. Kocsis, Huimei Liu, Qiang Luo, A. U. B. Wolter, and Shilong Zhang. The work at Peking University was supported by the National Basic Research Program of China (Grants No. 2021YFA1401900 and No. 2018YFA0305602) and the National Science

Foundation of China (Grants No. 12061131004, No. 11874069, and No. 11888101). The work at Brookhaven National Laboratory was supported by Office of Basic Energy Sciences (BES), Division of Materials Sciences and Engineering, U.S. Department of Energy (DOE), under Contract No. DE-SC0012704. X. L. further acknowledges support from China Postdoctoral Science Foundation (Grant No. 2020M680179). A portion of this research used resources at Spallation Neutron Source, a DOE Office of Science User Facility operated by the Oak Ridge National Laboratory. One of the neutron scattering experiments was performed at the Materials and Life Science Experimental Facility, J-PARC, Japan, under a user program (No. 2020B0148).

[1] L. Balents, *Spin Liquids in Frustrated Magnets*, Nature (London) **464**, 199 (2010).
[2] Y. Zhou, K. Kanoda, and T.-K. Ng, *Quantum Spin Liquid States*, Rev. Mod. Phys. **89**, 025003 (2017).
[3] C. Broholm, R. Cava, S. Kivelson, D. Nocera, M. Norman, and T. Senthil, *Quantum Spin Liquids*, Science **367**, eaay0668 (2020).
[4] A. Kitaev, *Anyons in an Exactly Solved Model and Beyond*, Ann. Phys. (Amsterdam) **321**, 2 (2006).
[5] G. Jackeli and G. Khaliullin, *Mott Insulators in the Strong Spin-Orbit Coupling Limit: From Heisenberg to a Quantum Compass and Kitaev Models*, Phys. Rev. Lett. **102**, 017205 (2009).
[6] H. Takagi, T. Takayama, G. Jackeli, G. Khaliullin, and S. E. Nagler, *Concept and Realization of Kitaev Quantum Spin Liquids*, Nat. Rev. Phys. **1**, 264 (2019).
[7] Y. Motome, R. Sano, S. Jang, Y. Sugita, and Y. Kato, *Materials Design of Kitaev Spin Liquids Beyond the Jackeli-Khaliullin Mechanism*, J. Phys. Condens. Matter **32**, 404001 (2020).
[8] S. Trebst and C. Hickey, *Kitaev Materials*, Phys. Rep. **950**, 1 (2022).
[9] J. Chaloupka, G. Jackeli, and G. Khaliullin, *Kitaev-Heisenberg Model on a Honeycomb Lattice: Possible Exotic Phases in Iridium Oxides* A_2IrO_3, Phys. Rev. Lett. **105**, 027204 (2010).
[10] K. W. Plumb, J. P. Clancy, L. J. Sandilands, V. V. Shankar, Y. F. Hu, K. S. Burch, H.-Y. Kee, and Y.-J. Kim, *α-$RuCl_3$: A Spin-Orbit Assisted Mott Insulator on a Honeycomb Lattice*, Phys. Rev. B **90**, 041112(R) (2014).
[11] H. Liu and G. Khaliullin, *Pseudospin Exchange Interactions in d^7 Cobalt Compounds: Possible Realization of the Kitaev Model*, Phys. Rev. B **97**, 014407 (2018).
[12] R. Sano, Y. Kato, and Y. Motome, *Kitaev-Heisenberg Hamiltonian for High-Spin d^7 Mott Insulators*, Phys. Rev. B **97**, 014408 (2018).
[13] H. Liu, J. Chaloupka, and G. Khaliullin, *Kitaev Spin Liquid in 3d Transition Metal Compounds*, Phys. Rev. Lett. **125**, 047201 (2020).
[14] C. Kim, H.-S. Kim, and J.-G. Park, *Spin-orbital Entangled State and Realization of Kitaev Physics in 3d Cobalt Compounds: A Progress Report*, J. Phys. Condens. Matter **34**, 023001 (2022).
[15] H. Liu, *Towards Kitaev Spin Liquid in 3d Transition Metal Compounds*, Int. J. Mod. Phys. B **35**, 2130006 (2021).
[16] L. Viciu, Q. Huang, E. Morosan, H. Zandbergen, N. Greenbaum, T. McQueen, and R. Cava, *Structure and Basic Magnetic Properties of the Honeycomb Lattice Compounds* $Na_2Co_2TeO_6$ *and* $Na_3Co_2SbO_6$, J. Solid State Chem. **180**, 1060 (2007).
[17] Y. Singh and P. Gegenwart, *Antiferromagnetic Mott Insulating State in Single Crystals of the Honeycomb Lattice Material* Na_2IrO_3, Phys. Rev. B **82**, 064412 (2010).
[18] X. Liu, T. Berlijn, W.-G. Yin, W. Ku, A. Tsvelik, Y.-J. Kim, H. Gretarsson, Y. Singh, P. Gegenwart, and J. P. Hill, *Long-Range Magnetic Ordering in* Na_2IrO_3, Phys. Rev. B **83**, 220403(R) (2011).
[19] R. D. Johnson, S. C. Williams, A. A. Haghighirad, J. Singleton, V. Zapf, P. Manuel, I. I. Mazin, Y. Li, H. O. Jeschke, R. Valentí, and R. Coldea, *Monoclinic Crystal Structure of α-$RuCl_3$ and the Zigzag Antiferromagnetic Ground State*, Phys. Rev. B **92**, 235119 (2015).
[20] R. Zhong, T. Gao, N. P. Ong, and R. J. Cava, *Weak-Field Induced Nonmagnetic State in a* Co*-Based Honeycomb*, Sci. Adv. **6**, eaay6953 (2020).
[21] I. Kimchi and Y.-Z. You, *Kitaev-Heisenberg-J_2-J_3 Model for the Iridates* A_2IrO_3, Phys. Rev. B **84**, 180407(R) (2011).
[22] J. Chaloupka, G. Jackeli, and G. Khaliullin, *Zigzag Magnetic Order in the Iridium Oxide* Na_2IrO_3, Phys. Rev. Lett. **110**, 097204 (2013).
[23] J. G. Rau, Eric Kin-Ho Lee, and H.-Y. Kee, *Generic Spin Model for the Honeycomb Iridates Beyond the Kitaev Limit*, Phys. Rev. Lett. **112**, 077204 (2014).
[24] Y. Sizyuk, C. Price, P. Wölfle, and N. B. Perkins, *Importance of Anisotropic Exchange Interactions in Honeycomb Iridates: Minimal Model for Zigzag Antiferromagnetic Order in* Na_2IrO_3, Phys. Rev. B **90**, 155126 (2014).
[25] Y. Yamaji, Y. Nomura, M. Kurita, R. Arita, and M. Imada, *First-Principles Study of the Honeycomb-Lattice Iridates* Na_2IrO_3 *in the Presence of Strong Spin-Orbit Interaction and Electron Correlations*, Phys. Rev. Lett. **113**, 107201 (2014).
[26] V. M. Katukuri, S. Nishimoto, V. Yushankhai, A. Stoyanova, H. Kandpal, S. Choi, R. Coldea, I. Rousochatzakis, L. Hozoi, and J. van den Brink, *Kitaev Interactions between $j = 1/2$ Moments in Honeycomb* Na_2IrO_3 *Are Large and Ferromagnetic: Insights from Ab Initio Quantum Chemistry Calculations*, New J. Phys. **16**, 013056 (2014).
[27] I. Rousochatzakis, J. Reuther, R. Thomale, S. Rachel, and N. B. Perkins, *Phase Diagram and Quantum Order by Disorder in the Kitaev $K_1 - K_2$ Honeycomb Magnet*, Phys. Rev. X **5**, 041035 (2015).
[28] J. Chaloupka and G. Khaliullin, *Magnetic Anisotropy in the Kitaev Model Systems* Na_2IrO_3 *and* $RuCl_3$, Phys. Rev. B **94**, 064435 (2016).
[29] J. Chaloupka and G. Khaliullin, *Hidden Symmetries of the Extended Kitaev-Heisenberg Model: Implications for the Honeycomb-Lattice Iridates* A_2IrO_3, Phys. Rev. B **92**, 024413 (2015).

[30] S. M. Winter, Y. Li, H. O. Jeschke, and R. Valentí, *Challenges in Design of Kitaev Materials: Magnetic Interactions from Competing Energy Scales*, Phys. Rev. B **93**, 214431 (2016).

[31] S.-H. Do, S.-Y. Park, J. Yoshitake, J. Nasu, Y. Motome, Y. S. Kwon, D. Adroja, D. Voneshen, K. Kim, T.-H. Jang, J.-H. Park, K.-Y. Choi, and S. Ji, *Majorana Fermions in the Kitaev Quantum Spin System* α-$RuCl_3$, Nat. Phys. **13**, 1079 (2017).

[32] Z. Wang *et al.*, *Pressure-Induced Melting of Magnetic Order and Emergence of a New Quantum State in* α-$RuCl_3$, Phys. Rev. B **97**, 245149 (2018).

[33] S. M. Winter, K. Riedl, D. Kaib, R. Coldea, and R. Valentí, *Probing* α-$RuCl_3$ *beyond Magnetic Order: Effects of Temperature and Magnetic Field*, Phys. Rev. Lett. **120**, 077203 (2018).

[34] A. Banerjee, P. Lampen-Kelley, J. Knolle, C. Balz, A. A. Aczel, B. Winn, Y. Liu, D. Pajerowski, J. Yan, C. A. Bridges, A. T. Savici, B. C. Chakoumakos, M. D. Lumsden, D. A. Tennant, R. Moessner, D. G. Mandrus, and S. E. Nagler, *Excitations in the Field-Induced Quantum Spin Liquid State of* α-$RuCl_3$, npj Quantum Mater. **3**, 8 (2018).

[35] J. S. Gordon, A. Catuneanu, E. S. Sørensen, and H.-Y. Kee, *Theory of the Field-Revealed Kitaev Spin Liquid*, Nat. Commun. **10**, 2470 (2019).

[36] C. Hickey and S. Trebst, *Emergence of a Field-Driven* $U(1)$ *Spin Liquid in the Kitaev Honeycomb Model*, Nat. Commun. **10**, 530 (2019).

[37] W. Yao and Y. Li, *Ferrimagnetism and Anisotropic Phase Tunability by Magnetic Fields in* $Na_2Co_2TeO_6$, Phys. Rev. B **101**, 085120 (2020).

[38] C. Wong, M. Avdeev, and C. D. Ling, *Zig-zag Magnetic Ordering in Honeycomb-Layered* $Na_3Co_2SbO_6$, J. Solid State Chem. **243**, 18 (2016).

[39] J.-Q. Yan, S. Okamoto, Y. Wu, Q. Zheng, H. D. Zhou, H. B. Cao, and M. A. McGuire, *Magnetic Order in Single Crystals of* $Na_3Co_2SbO_6$ *with a Honeycomb Arrangement of* $3d^7$ Co^{2+} *Ions*, Phys. Rev. Mater. **3**, 074405 (2019).

[40] M. I. Stratan, I. L. Shukaev, T. M. Vasilchikova, A. N. Vasiliev, A. N. Korshunov, A. I. Kurbakov, V. B. Nalbandyan, and E. A. Zvereva, *Synthesis, Structure and Magnetic Properties of Honeycomb-Layered* $Li_3Co_2SbO_6$ *with New Data on Its Sodium Precursor,* $Na_3Co_2SbO_6$, New J. Chem. **43**, 13545 (2019).

[41] W. Wang, Z.-Y. Dong, S.-L. Yu, and J.-X. Li, *Theoretical Investigation of Magnetic Dynamics in* α-$RuCl_3$, Phys. Rev. B **96**, 115103 (2017).

[42] L. Janssen, E. C. Andrade, and M. Vojta, *Magnetization Processes of Zigzag States on the Honeycomb Lattice: Identifying Spin Models for* α-$RuCl_3$ *and* Na_2IrO_3, Phys. Rev. B **96**, 064430 (2017).

[43] J. Rusnačko, D. Gotfryd, and J. Chaloupka, *Kitaev-like Honeycomb Magnets: Global Phase Behavior and Emergent Effective Models*, Phys. Rev. B **99**, 064425 (2019).

[44] P. A. Maksimov and A. L. Chernyshev, *Rethinking* α-$RuCl_3$, Phys. Rev. Res. **2**, 033011 (2020).

[45] P. Laurell and S. Okamoto, *Dynamical and Thermal Magnetic Properties of the Kitaev Spin Liquid Candidate* α-$RuCl_3$, npj Quantum Mater. **5**, 2 (2020).

[46] H. B. Cao, A. Banerjee, J.-Q. Yan, C. A. Bridges, M. D. Lumsden, D. G. Mandrus, D. A. Tennant, B. C. Chakoumakos, and S. E. Nagler, *Low-Temperature Crystal and Magnetic Structure of* α-$RuCl_3$, Phys. Rev. B **93**, 134423 (2016).

[47] W. Chen, X. Li, Z. Hu, Z. Hu, L. Yue, R. Sutarto, F. He, K. Iida, K. Kamazawa, W. Yu, X. Lin, and Y. Li, *Spin-Orbit Phase Behavior of* $Na_2Co_2TeO_6$ *at Low Temperatures*, Phys. Rev. B **103**, L180404 (2021).

[48] C. H. Lee, S. Lee, Y. S. Choi, Z. H. Jang, R. Kalaivanan, R. Sankar, and K.-Y. Choi, *Multistage Development of Anisotropic Magnetic Correlations in the* Co*-Based Honeycomb Lattice* $Na_2Co_2TeO_6$, Phys. Rev. B **103**, 214447 (2021).

[49] M. Songvilay, J. Robert, S. Petit, J. A. Rodriguez-Rivera, W. D. Ratcliff, F. Damay, V. Balédent, M. Jiménez-Ruiz, P. Lejay, E. Pachoud, A. Hadj-Azzem, V. Simonet, and C. Stock, *Kitaev Interactions in the* Co *Honeycomb Antiferromagnets* $Na_3Co_2SbO_6$ *and* $Na_2Co_2TeO_6$, Phys. Rev. B **102**, 224429 (2020).

[50] G. Lin *et al.*, *Field-Induced Quantum Spin Disordered State in Spin-*$1/2$ *Honeycomb Magnet* $Na_2Co_2TeO_6$, Nat. Commun. **12**, 5559 (2021).

[51] C. Kim, J. Jeong, G. Lin, P. Park, T. Masuda, S. Asai, S. Itoh, H.-S. Kim, H. Zhou, J. Ma, and J.-G. Park, *Antiferromagnetic Kitaev Interaction* $J_{\mathrm{eff}} = 1/2$ *Cobalt Honeycomb Materials* $Na_3Co_2SbO_6$ *and* $Na_2Co_2TeO_6$, J. Phys. Condens. Matter **34**, 045802 (2022).

[52] A. M. Samarakoon, Q. Chen, H. Zhou, and V. O. Garlea, *Static and Dynamic Magnetic Properties of Honeycomb Lattice Antiferromagnets* $Na_2M_2TeO_6$, $M =$ Co *and* Ni, Phys. Rev. B **104**, 184415 (2021).

[53] A. L. Sanders, R. A. Mole, J. Liu, A. J. Brown, D. Yu, C. D. Ling, and S. Rachel, *Dominant Kitaev Interactions in the Honeycomb Materials* $Na_3Co_2SbO_6$ *and* $Na_2Co_2TeO_6$, Phys. Rev. B **106**, 014413 (2022).

[54] W. Yao, K. Iida, K. Kamazawa, and Y. Li, *Excitations in the Ordered and Paramagnetic States of Honeycomb Magnet* $Na_2Co_2TeO_6$, Phys. Rev. Lett. **129**, 147202 (2022).

[55] P. Lampen-Kelley, S. Rachel, J. Reuther, J.-Q. Yan, A. Banerjee, C. A. Bridges, H. B. Cao, S. E. Nagler, and D. Mandrus, *Anisotropic Susceptibilities in the Honeycomb Kitaev System* α-$RuCl_3$, Phys. Rev. B **98**, 100403(R) (2018).

[56] C. Balz, L. Janssen, P. Lampen-Kelley, A. Banerjee, Y. H. Liu, J.-Q. Yan, D. G. Mandrus, M. Vojta, and S. E. Nagler, *Field-Induced Intermediate Ordered Phase and Anisotropic Interlayer Interactions in* α-$RuCl_3$, Phys. Rev. B **103**, 174417 (2021).

[57] V. Kocsis, D. A. S. Kaib, K. Riedl, S. Gass, P. Lampen-Kelley, D. G. Mandrus, S. E. Nagler, N. Pérez, K. Nielsch, B. Büchner, A. U. B. Wolter, and R. Valentí, *Magnetoelastic Coupling Anisotropy in the Kitaev Material* α-$RuCl_3$, Phys. Rev. B **105**, 094410 (2022).

[58] See Supplemental Material at http://link.aps.org/supplemental/10.1103/PhysRevX.12.041024 for additional methods, data, and analyses, which includes additional Refs. [59–63].

[59] C.-M. Wu, G. Deng, J. Gardner, P. Vorderwisch, W.-H. Li, S. Yano, J.-C. Peng, and E. Imamovic, *SIKA—The Multiplexing Cold-Neutron Triple-Axis Spectrometer at ANSTO*, J. Instrum. **11**, P10009 (2016).

[60] B. Winn, U. Filges, V. O. Garlea, M. Graves-Brook, M. Hagen, C. Jiang, M. Kenzelmann, L. Passell, S. M. Shapiro, X. Tong, and I. Zaliznyak, *Recent Progress on HYSPEC, and Its Polarization Analysis Capabilities*, EPJ Web Conf. **83**, 03017 (2015).

[61] R. Kajimoto *et al.*, *The Fermi Chopper Spectrometer 4SEASONS at J-PARC*, J. Phys. Soc. Jpn. **80**, SB025 (2011).

[62] Y. Inamura, T. Nakatani, J. Suzuki, and T. Otomo, *Development Status of Software "Utsusemi" for Chopper Spectrometers at MLF, J-PARC*, J. Phys. Soc. Jpn. **82**, SA031 (2013).

[63] R. Ewings, A. Buts, M. Le, J. van Duijn, I. Bustinduy, and T. Perring, *Horace: Software for the Analysis of Data from Single Crystal Spectroscopy Experiments at Time-of-Flight Neutron Instruments*, Nucl. Instrum. Methods Phys. Res., Sect. A **834**, 132 (2016).

[64] J. A. Sears, Y. Zhao, Z. Xu, J. W. Lynn, and Y.-J. Kim, *Phase Diagram of* α-$RuCl_3$ *in an In-Plane Magnetic Field*, Phys. Rev. B **95**, 180411(R) (2017).

[65] V. Hardy, M. R. Lees, O. A. Petrenko, D. M. Paul, D. Flahaut, S. Hébert, and A. Maignan, *Temperature and Time Dependence of the Field-Driven Magnetization Steps in* $Ca_3Co_2O_6$ *Single Crystals*, Phys. Rev. B **70**, 064424 (2004).

[66] H. Ueda, H. A. Katori, H. Mitamura, T. Goto, and H. Takagi, *Magnetic-Field Induced Transition to the* $1/2$ *Magnetization Plateau State in the Geometrically Frustrated Magnet* $CdCr_2O_4$, Phys. Rev. Lett. **94**, 047202 (2005).

[67] G. Cao, V. Durairaj, S. Chikara, S. Parkin, and P. Schlottmann, *Partial Antiferromagnetism in Spin-Chain* $Sr_5Rh_4O_{12}$, $Ca_5Ir_3O_{12}$, *and* Ca_4IrO_6 *Single Crystals*, Phys. Rev. B **75**, 134402 (2007).

[68] Y. J. Jo, S. Lee, E. S. Choi, H. T. Yi, W. Ratcliff, Y. J. Choi, V. Kiryukhin, S. W. Cheong, and L. Balicas, $3:1$ *Magnetization Plateau and Suppression of Ferroelectric Polarization in an Ising Chain Multiferroic*, Phys. Rev. B **79**, 012407 (2009).

[69] K. A. Ross, J. P. C. Ruff, C. P. Adams, J. S. Gardner, H. A. Dabkowska, Y. Qiu, J. R. D. Copley, and B. D. Gaulin, *Two-Dimensional Kagome Correlations and Field Induced Order in the Ferromagnetic XY Pyrochlore* $Yb_2Ti_2O_7$, Phys. Rev. Lett. **103**, 227202 (2009).

[70] J. D. Thompson, P. A. McClarty, H. M. Rønnow, L. P. Regnault, A. Sorge, and M. J. P. Gingras, *Rods of Neutron Scattering Intensity in* $Yb_2Ti_2O_7$*: Compelling Evidence for Significant Anisotropic Exchange in a Magnetic Pyrochlore Oxide*, Phys. Rev. Lett. **106**, 187202 (2011).

[71] A. Scheie, J. Kindervater, S. Zhang, H. J. Changlani, G. Sala, G. Ehlers, A. Heinemann, G. S. Tucker, S. M. Koohpayeh, and C. Broholm, *Multiphase Magnetism in* $Yb_2Ti_2O_7$, Proc. Natl. Acad. Sci. U.S.A. **117**, 27245 (2020).

[72] A. Scheie, O. Benton, M. Taillefumier, L. D. Jaubert, G. Sala, N. Jalarvo, S. M. Koohpayeh, and N. Shannon, *Dynamical Scaling as a Signature of Multiple Phase Competition in* $Yb_2Ti_2O_7$, arXiv:2202.11085.

[73] J. Zheng, K. Ran, T. Li, J. Wang, P. Wang, B. Liu, Z.-X. Liu, B. Normand, J. Wen, and W. Yu, *Gapless Spin Excitations in the Field-Induced Quantum Spin Liquid Phase of* α-$RuCl_3$, Phys. Rev. Lett. **119**, 227208 (2017).

[74] A. U. B. Wolter, L. T. Corredor, L. Janssen, K. Nenkov, S. Schönecker, S.-H. Do, K.-Y. Choi, R. Albrecht, J. Hunger, T. Doert, M. Vojta, and B. Büchner, *Field-Induced Quantum Criticality in the Kitaev System* α-$RuCl_3$, Phys. Rev. B **96**, 041405(R) (2017).

[75] I. A. Leahy, C. A. Pocs, P. E. Siegfried, D. Graf, S.-H. Do, K.-Y. Choi, B. Normand, and M. Lee, *Anomalous Thermal Conductivity and Magnetic Torque Response in the Honeycomb Magnet* α-$RuCl_3$, Phys. Rev. Lett. **118**, 187203 (2017).

[76] S.-H. Baek, S.-H. Do, K.-Y. Choi, Y. S. Kwon, A. U. B. Wolter, S. Nishimoto, J. van den Brink, and B. Büchner, *Evidence for a Field-Induced Quantum Spin Liquid in* α-$RuCl_3$, Phys. Rev. Lett. **119**, 037201 (2017).

[77] Y. J. Yu, Y. Xu, K. J. Ran, J. M. Ni, Y. Y. Huang, J. H. Wang, J. S. Wen, and S. Y. Li, *Ultralow-Temperature Thermal Conductivity of the Kitaev Honeycomb Magnet* α-$RuCl_3$ *across the Field-Induced Phase Transition*, Phys. Rev. Lett. **120**, 067202 (2018).

[78] C. Wellm, J. Zeisner, A. Alfonsov, A. U. B. Wolter, M. Roslova, A. Isaeva, T. Doert, M. Vojta, B. Büchner, and V. Kataev, *Signatures of Low-Energy Fractionalized Excitations in* α-$RuCl_3$ *from Field-Dependent Microwave Absorption*, Phys. Rev. B **98**, 184408 (2018).

[79] Y. Kasahara, T. Ohnishi, Y. Mizukami, O. Tanaka, S. Ma, K. Sugii, N. Kurita, H. Tanaka, J. Nasu, Y. Motome, T. Shibauchi, and Y. Matsuda, *Majorana Quantization and Half-Integer Thermal Quantum Hall Effect in a Kitaev Spin Liquid*, Nature (London) **559**, 227 (2018).

[80] A. Sahasrabudhe, D. A. S. Kaib, S. Reschke, R. German, T. C. Koethe, J. Buhot, D. Kamenskyi, C. Hickey, P. Becker, V. Tsurkan, A. Loidl, S. H. Do, K. Y. Choi, M. Grüninger, S. M. Winter, Z. Wang, R. Valentí, and P. H. M. van Loosdrecht, *High-Field Quantum Disordered State in* α-$RuCl_3$*: Spin Flips, Bound States, and Multiparticle Continuum*, Phys. Rev. B **101**, 140410(R) (2020).

[81] T. Yokoi, S. Ma, Y. Kasahara, S. Kasahara, T. Shibauchi, N. Kurita, H. Tanaka, J. Nasu, Y. Motome, C. Hickey, S. Trebst, and Y. Matsuda, *Half-Integer Quantized Anomalous Thermal Hall Effect in the Kitaev Material Candidate* α-$RuCl_3$, Science **373**, 568 (2021).

[82] A. M. Samarakoon, G. Wachtel, Y. Yamaji, D. A. Tennant, C. D. Batista, and Y. B. Kim, *Classical and Quantum Spin Dynamics of the Honeycomb* Γ *Model*, Phys. Rev. B **98**, 045121 (2018).

[83] P. Saha, Z. Fan, D. Zhang, and G.-W. Chern, *Hidden Plaquette Order in a Classical Spin Liquid Stabilized by Strong Off-Diagonal Exchange*, Phys. Rev. Lett. **122**, 257204 (2019).

[84] Q. Luo, J. Zhao, H.-Y. Kee, and X. Wang, *Gapless Quantum Spin Liquid in a Honeycomb* Γ *Magnet*, npj Quantum Mater. **6**, 57 (2021).